Journal of Materials Chemistry C

Green Synthesis of Reduced Ti3C2Tx MXene Nanosheets with Enhanced Conductivity, Oxidation Stability, and SERS Activity

Journal:	*Journal of Materials Chemistry C*
Manuscript ID	TC-ART-12-2019-006984.R1
Article Type:	Paper
Date Submitted by the Author:	28-Feb-2020
Complete List of Authors:	Limbu, Tej; North Carolina Central University, Chemistry and Biochemistry Chitara, Basant; North Carolina Central University, Chemistry & Biochemistry Orlando, Jason; North Carolina Central University Garcia Cervantes, Martha; North Carolina Central University, Chemistry & Biochemistry Kumari, Shalini; Pennsylvania State University University Park, Department of Physics Li, Qi; Pennsylvania State University University Park, Department of Physics Tang, Yongan ; North Carolina Central University, Department of Mathematics and Physics Yan, Fei; North Carolina Central University, Chemistry & Biochemistry

Green Synthesis of Reduced $Ti_3C_2T_x$ MXene Nanosheets with Enhanced Conductivity, Oxidation Stability, and SERS Activity

Tej B. Limbu,[†] *Basant Chitara,*[†] *Jason D. Orlando,*[†] *Martha Y. Garcia Cervantes,*[†] *Shalini Kumari,*[‖] *Qi Li,*[‖] *Yongan Tang,*[‡] *Fei Yan*,*[†]

[†]Department of Chemistry and Biochemistry, North Carolina Central University, Durham, NC 27707, USA

[‡]Department of Mathematics and Physics, North Carolina Central University, Durham, NC 27707, USA

[‖]Department of Physics, The Pennsylvania State University, University Park, PA 16802, USA

KEYWORDS. MXene nanosheets, reduction process, enhanced conductivity and oxidation stability, SERS.

ABSTRACT

Transition metal carbides (MXenes) are an emerging family of highly conductive two-dimensional materials with additional functional properties introduced by surface terminations. Further modification of the surface terminations makes MXenes even more appealing for practical applications. Herein, we report a facile and environmentally benign synthesis of reduced $Ti_3C_2T_x$ MXene (r-$Ti_3C_2T_x$) via a simple treatment with L-ascorbic acid at room temperature. r-$Ti_3C_2T_x$ shows a six-fold increase in the electrical conductivity, from 471 ± 49 for regular $Ti_3C_2T_x$ to 2819 ± 306 S/m for the reduced version. Additionally, we show an enhanced oxidation stability

of r-$Ti_3C_2T_x$ as compared to regular $Ti_3C_2T_x$. An examination of the surface-enhanced Raman scattering (SERS) activity reveals that the SERS enhancement factor of r-$Ti_3C_2T_x$ is an order of magnitude higher than that of regular $Ti_3C_2T_x$. The improved SERS activity of r-$Ti_3C_2T_x$ is attributed to the charge transfer interaction between the MXene surface and probe molecules, re-enforced by increased electronic density of states (DOS) at the Fermi level of r-$Ti_3C_2T_x$. The findings of this study suggest that reduced MXene could be a superior choice over regular MXene, especially for the applications that employ high electronic conductivity, such as electrode materials for batteries and supercapacitors, photodetectors, and SERS-based sensors.

1. INTRODUCTION

Since its discovery in 2011,[1] titanium carbides also called MXenes, a two-dimensional (2D) layered material, have attracted increasing attention from the scientific community, due to its exciting properties such as high metallic-like conductivity, good environmental and chemical stability, and controllable surface hydrophilicity.[2,3] Subsequently, several other species of the MXene family[4–8] have been discovered and synthesized in laboratories by top-down approaches starting with a three-dimensional parent material known as MAX. MAX phases are transition metal carbides, nitrides, or carbonitrides with the general formula $M_{n+1}AX_n$, where n = 1,2, or 3, M is a transition metal, A is an A group element (mainly 13 and 14 group), and X is C and/or N. After removal of the A layers in MAX phases by chemical etching, the obtained 2D materials are regarded as MXenes, which are usually represented by general formula $M_{n+1}X_nT_x$, where T_x is the surface termination acquired during the chemical etching process. Depending upon the type of M and X elements, and surface terminations, various members of the MXene family are known to exhibit quite different physical properties and chemical behavior; from metallic to semiconducting,

or topological insulators, and even magnetic.[6,7,9] Due to their diverse and exciting properties, MXenes have been explored for a myriad of applications, these include energy storage devices,[10–12] catalysis,[5,13,14] water desalination,[15] transparent conductors,[16,17] light absorbers,[3] electromagnetic interference shielding,[18] photodetection,[19] and surface-enhanced Raman scattering (SERS) detection,[4,20,21] among others.

Among a wide variety of MXene species, $Ti_3C_2T_x$ MXene is reported to have shown the highest electrical conductivity[22] and has been studied most extensively. It possesses impressive metallic-like conductivity comparable to those of reduced graphene oxide (GO) and carbon nanotubes, [23,24] and for most applications, such as electrode materials for batteries, supercapacitors, transparent conductors, plasmonic devices, photodetectors, and SERS substrates, high electrical conductivity is desired. Interestingly, the conductivity of MXenes can be further increased by de-intercalation and surface de-functionalization.[6] Hart et al.[6] demonstrated by in situ vacuum annealing, electrical biasing, and spectroscopic analysis in transmission electron microscopy (TEM) that loss of -OH and -F terminations in $Ti_3C_2T_x$ MXene improves electronic conductivity. This result is consistent with the literature report.[25] which by density functional theory simulation showed that surface functionalization with -OH, -H, -F, and -O on Ti_3C_2 MXene reduces the density of states (DOS) at the Fermi level, thereby reducing the conductivity. This implies that there exists a plenty of room for further enhancement of the electrical conductivity of MXene by surface modification. Reduction of MXenes could be a new approach to tailor the properties and conductivity enhancement, in analogy with the reduction of insulating GO to highly conducting reduced-graphene oxide (r-GO).[26,27] Yoon et al.[2] showed that Li-ethylenediamine (Li-EDA) treatment on $Ti_3C_2T_x$ removes most of the F and OH terminations and Ti^{4+} chemical states are changed to Ti^{3+}, and the reduction of $Ti_3C_2T_x$ MXene produces Pauli paramagnetic character.

Although this work showed an effective method of $Ti_3C_2T_x$ MXene reduction, the use of Li-EDA as a reducing agent required a glove-box environment for safety purposes. This indicates a need of a safer, reproducible, and easily accessible method of the MXene reduction process.

Among several potential applications, MXenes have shown promise for making cheap and efficient SERS substrates.[4,20,21,28] SERS is a non-destructive and highly sensitive technique of molecular detection present at a trace amount. Although noble metal nanostructure-based SERS substrates have shown an ultrahigh enhancement factor (EF) of 10^{14},[29] the high cost of production limits their wide use for practical purposes. MXenes, which are produced by simple solution processing methods with relatively cheap precursors, can be an alternative material for commercial SERS substrates. Sarycheva et al.[20] showed that $Ti_3C_2T_x$ MXene-based SERS substrates enhanced the Raman signal of common organic dyes as high as 10^6. Soundiraraju et al.[4] reported even more interesting SERS results with titanium nitride (Ti_2NT_x) MXene. They found an EF of 10^{12} using rhodamine 6G as a probe compound on SERS substrate made by coating a paper with Ti_2NT_x. Such a high EF is good enough for single molecule detection, indicating a potential use of MXenes for replacing expensive SERS substrates made from noble metal nanostructures.

Despite their exciting physical and electrochemical properties, it is widely known that MXenes have a weak chemical and environmental stability,[30–35] which can limit their use for practical applications. Because of the spontaneous and rapid oxidation issue in water and air, better ways of storing MXenes have also been explored and suggested.[30,32,35] However, it would be even more interesting if the cause of oxidation would be identified and the MXene crystals would be engineered to make them shelf-stable, or one would discover a state-of-the-art route to synthesize chemically and environmentally stable MXenes.

In this work, we demonstrate a green protocol for room temperature synthesis of reduced $Ti_3C_2T_x$ MXene (r-$Ti_3C_2T_x$) via a simple L-ascorbic acid treatment, which is facile and highly reproducible. We show a significant modification of the properties in r-$Ti_3C_2T_x$ with enhanced electrical conductivity and oxidation stability as compared to that of $Ti_3C_2T_x$ MXene ($Ti_3C_2T_x$) prepared by conventional methods,[1,20,36] showing reduced MXene as a primary choice for using in several applications that employ high electronic conductivity. We also report an application of r-$Ti_3C_2T_x$ as a SERS substrate and demonstrate an improvement in the SERS EF by an order of magnitude compared to that of $Ti_3C_2T_x$.

2. EXPERIMENTAL SECTION

2.*1 Synthesis of $Ti_3C_2T_x$*

To synthesize r-$Ti_3C_2T_x$, we started with etching of Al layers in Ti_3AlC_2 MAX powder purchased from Carbon-Ukraine (Y-Carbon, Ltd.). The reduction process is preceded by etching and MXene delamination. The etching of Al layers and delamination of MXene were carried out following the methods described in the report[36] with a slight modification. Briefly, 0.5 g of Ti_3AlC_2 MAX powder was slowly added to 10 ml of 30% hydrofluoric acid (HF) (ACROS Organics, 48-51% solution in water) under a gentle and constant stirring condition with the help of a Teflon magnetic bar, and the stirring was continued for 7 hours. The solution was then washed one time with deionized (DI) water by centrifugation at a speed of 3500 rpm for 30 minutes and water like supernatant was removed. The sediment was then further washed with at least 5 liters of DI water via vacuum-assisted filtration using a polyvinyl difluoride (PVDF) filter membrane with 0.22 μm of pore size (Durapore, Millipore) until the pH of the filtrate was lowered to ~6.5. The cleaned sediment was then dried in the same filter cup by placing it in a vacuum desiccator for 24 hours. For the delamination process, 100 mg of $Ti_3C_2T_x$ powder was put into 20 ml of 1%

tetramethylammonium hydroxide (TMAOH) (Alfa Aesar, Electronic Grade, 99.9999% (metal basis) liquid) solution and was shaken for 24 hours. After 24 hours of shaking, the solution was centrifuged at 5000 rpm for 30 minutes to separate out the unwanted brown solution containing TMAOH. The centrifugation process was repeated several times until the pH of the supernatant solution was decreased to ~7. The MXene solution was then centrifuged at 3500 rpm for 5 minutes to separate out the bigger and unetched particles, and the stable MXene colloidal solution was collected for further processing.

2.2 Green Synthesis of r-$Ti_3C_2T_x$

For the reduction process, first, DI water was added to the obtained MXene colloidal solution to make a total volume of 40 ml. The solution was shaken and divided into two equal volumes, 20 ml each for $Ti_3C_2T_x$ and r-$Ti_3C_2T_x$. One part was further centrifuged to extract a slurry and freeze-dried to obtain powder material for characterizations. The obtained $Ti_3C_2T_x$ powder was weighed to be $\sim 25\ mg$. The other part, which was expected to contain the same amount of $Ti_3C_2T_x$ ($\sim 25\ mg$) in 20 ml of water was mixed with 1 g of L-ascorbic acid (Fisher Scientific, Reagent Grade) and shaken for 5 hours. After 5 hours of treatment with L-ascorbic acid, the solution was centrifuged several times at 5000 rpm for 30 minutes to remove the acidic solution. Finally, a slurry of r-$Ti_3C_2T_x$ nanosheets was extracted and freeze-dried to obtain r-$Ti_3C_2T_x$ powder for characterizations. In order to obtain $Ti_3C_2T_x$ and r-$Ti_3C_2T_x$ colloidal solutions for film preparation on SiO_2/Si and paper, the synthesis process was repeated, and instead of freeze-drying, the slurries of MXene nanosheets were dissolved in a suitable amount of methanol.

2.3 *Fabrication of $Ti_3C_2T_x$/r-$Ti_3C_2T_x$ Films*

To fabricate the films of $Ti_3C_2T_x$ and r-$Ti_3C_2T_x$ on SiO_2/Si substrates, the slurries of $Ti_3C_2T_x$ and r-$Ti_3C_2T_x$ nanosheets were dissolved in a suitable amount of methanol separately in

two different glass vials to obtain dense colloidal solutions. The dense colloidal solutions of $Ti_3C_2T_x$ and r-$Ti_3C_2T_x$ nanosheets were drop casted on oxygen plasma-cleaned SiO_2/Si substrates followed by subsequent heating at 60 ^oC by placing the samples on a hot plate. $Ti_3C_2T_x$ and r-$Ti_3C_2T_x$ films on paper substrates were fabricated on PVDF filter papers with a pore size of 0.22 μm (Durapore, Millipore) employing vacuum-assisted filtration.

2.4 Characterization of $Ti_3C_2T_x$/r-$Ti_3C_2T_x$

Characterization of $Ti_3C_2T_x$/r-$Ti_3C_2T_x$ samples were performed by using Raman spectroscopy (Horiba LabRAM Evolution RAMAN microscope), atomic force microscopy (AFM) (Horiba Smart SPM Atomic Force Microscope), UV-visible spectroscopy (VWR, UV-3100PC Spectrophotometer), scanning electron microscopy (SEM) (FEI Verios 460L), TEM (FEI Talos F200X, 200 KV accelerating voltage), X-ray diffractometry (XRD) (Rigaku SmartLab X-ray Diffractometer), and X-ray photoelectron spectroscopy (XPS) (SPECS FlexMod XPS, Mg kα excitation (1254 eV)). Ti(20 nm)/Au(300 nm) contact pads were deposited on the fabricated MXene films by using electron beam evaporation. Electrical properties were studied by employing transmission line measurements with two probes in a probe station (EVERBEING) equipped with a Keithley analyzer (4200A-SCS). For the test of oxidation stability, the dried and stored $Ti_3C_2T_x$ and r-$Ti_3C_2T_x$ powders were re-dispersed in water at a concentration of 15 mg/10 ml, sonicated for 10 minutes and left open to ambient for several days. The stability test was repeated with another concentration, 5 mg/10 ml of water for confirmation. The SERS measurements were performed with a Raman spectrometer (Horiba LabRAM Evolution RAMAN microscope) by using a 532 nm of laser excitation and 100× objective lens with an integration time of 20 s. Raman enhancement of the $Ti_3C_2T_x$ and r-$Ti_3C_2T_x$ was examined with three dye molecules, i.e., crystal violet (CV)

(ACROS Organics), methylene blue (MB) (ACROS Organics), and rhodamine 6G (R6G) (ACROS Organics).

3. RESULTS AND DISCUSSION

3.1 Synthesis and Characterization

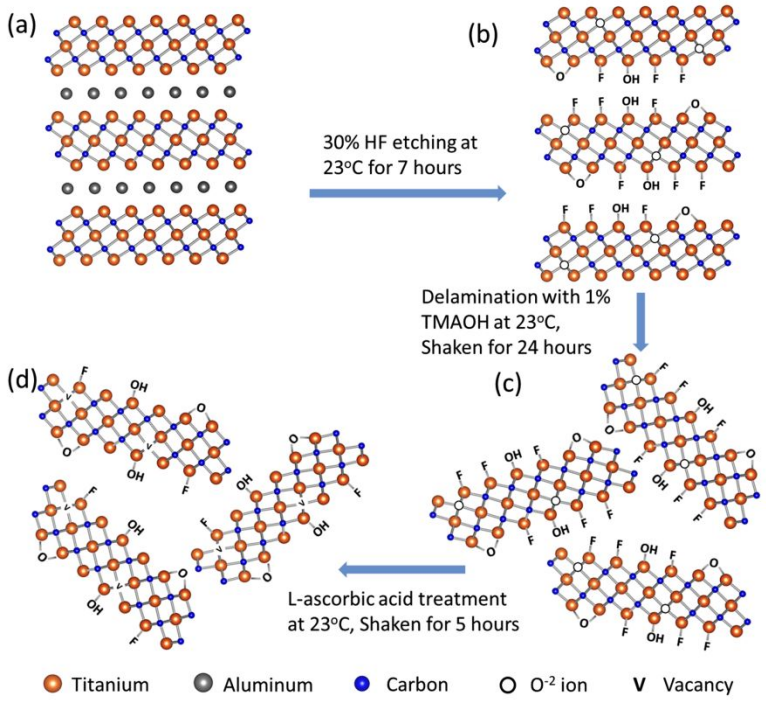

Figure 1. Schematic diagram of r-$Ti_3C_2T_x$ synthesis

Figure 1 schematically summarizes the synthesis route for r-$Ti_3C_2T_x$. Etching of Al layers in Ti_3AlC_2 MAX phase (Figure 1a) with HF produces 2D crystals of titanium carbide with -O, -OH, and -F terminations (Figure 2b). The $Ti_3C_2T_x$ layers are still bound to each other by a weak hydrogen or van der Waals force between T_x (OH, F, O) terminations of two adjacent MXene layers.[1,36] Upon intercalation with tetramethylammonium ions during delamination using TMAOH, the $Ti_3C_2T_x$ layers are separated into free standing particles (Figure 1c). Treatment of

colloidal $Ti_3C_2T_x$ solution with L-ascorbic acid changes the surface chemistry of MXene nanosheets to give rise to reduced $Ti_3C_2T_x$ (Figure 1d). We note that we have followed the model presented by Yoon et al.[2] to describe the surface chemistry changes in the 2D $Ti_3C_2T_x$ due to HF etching and reduction processes as depicted in Figures 1b, 1c, and 1d, which will be discussed later in detail.

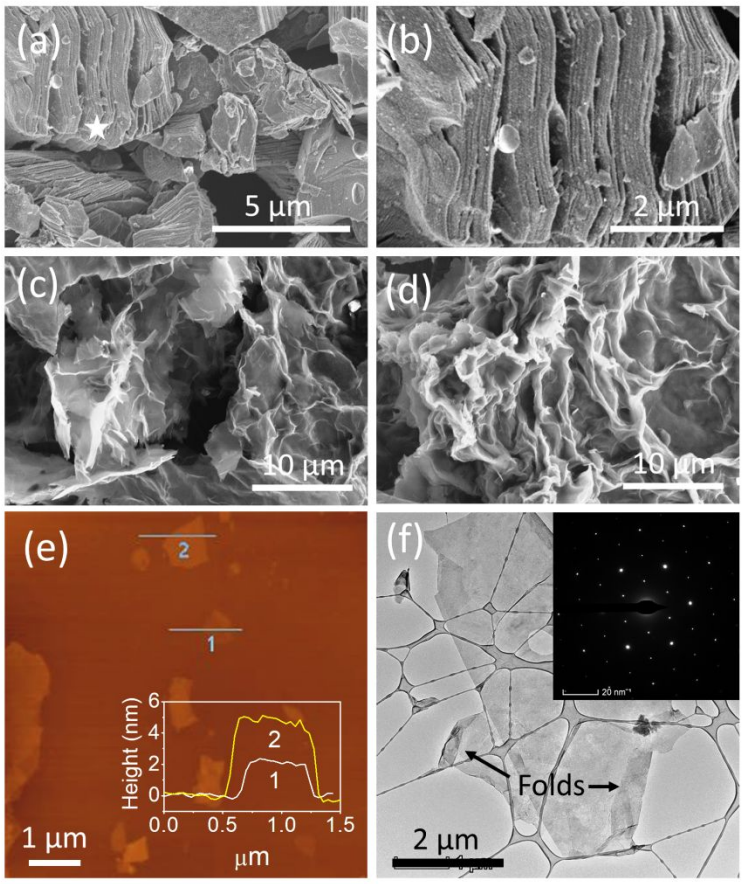

Figure 2. (a,b) SEM micrographs of $Ti_3C_2T_x$ after HF-etching of Ti_3AlC_2 MAX phase, (c,d) SEM micrographs of $Ti_3C_2T_x$ and r-$Ti_3C_2T_x$ powders, respectively, (e) Tapping mode AFM image of $Ti_3C_2T_x$ nanosheets on SiO_2/Si, and (f) High magnification TEM image of a $Ti_3C_2T_x$ nanosheet suspended over holy carbon grid. The inset shows the selected area electron diffraction (SAED) pattern.

SEM images in Figure 2a and 2b show that 3D Ti_3AlC_2 MAX particles are changed to accordion-like multilayer $Ti_3C_2T_x$ structures indicating that Al layers in Ti_3AlC_2 MAX phase are etched out by HF. Figures 2c and 2d show fabric-like SEM micrographs of $Ti_3C_2T_x$ powder before and after L-ascorbic acid treatment, respectively. Tapping mode AFM image (Figure 2e) of $Ti_3C_2T_x$ nanosheets deposited onto SiO_2/Si substrates show that majority of the sheets are large with a lateral dimension of about 1 μm and 2 to 6 nm height corresponding to 1 to 3 layers. Figure 1f shows a high magnification TEM image of a 2D $Ti_3C_2T_x$ nanosheet suspended over a holy carbon grid, and its inset shows the selected area electron diffraction with a six-fold reflection spots corresponding to hexagonal crystal symmetry of $Ti_3C_2T_x$.

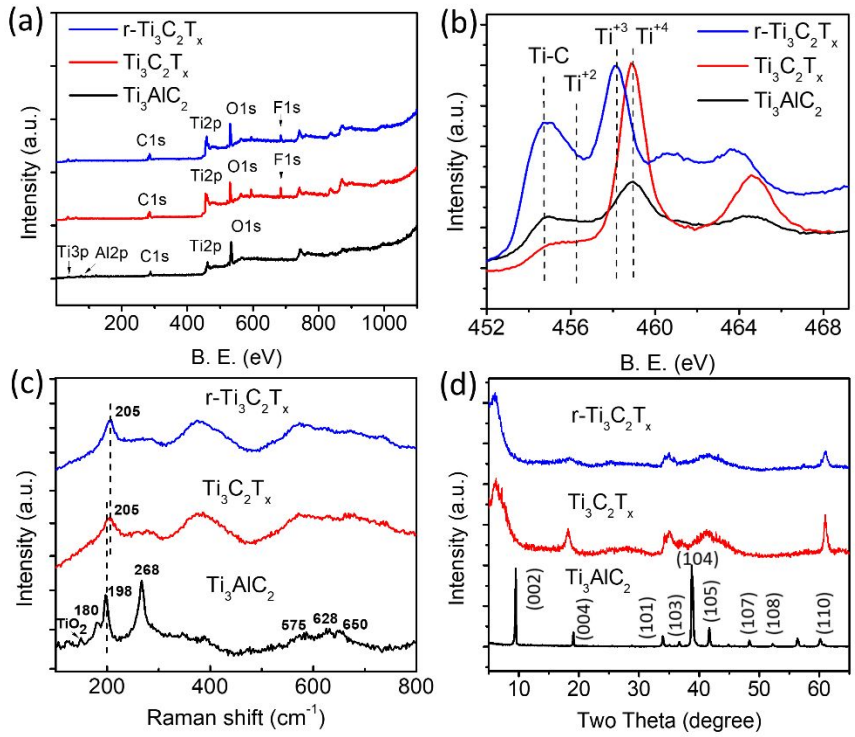

Figure 3. (a) XPS survey spectra, (b) high resolution XPS spectra of Ti2p region, (c) Raman spectra, and (d) XRD spectra, respectively, of Ti_3AlC_2 MAX phase (black), $Ti_3C_2T_x$ (red), and r-$Ti_3C_2T_x$ (blue)

XPS analysis of the samples shows a clear difference among Ti_3AlC_2 MAX phase, $Ti_3C_2T_x$, and r-$Ti_3C_2T_x$. XPS survey spectrum (Figure 3a) of Ti_3AlC_2 MAX phase (black) shows a peak at 77.0 eV corresponding to Al, which however, is below the detection limit in the spectra of $Ti_3C_2T_x$ (red), and r-$Ti_3C_2T_x$ (blue). This indicates that HF treatment on Ti_3AlC_2 MAX powder removes out most of the Al layers. The survey spectra of $Ti_3C_2T_x$ shows a F peak at 685.0 eV with 8.1 atomic %, due to the addition of fluorine during HF etching process.[36] After treatment with L-ascorbic acid, fluorine amount significantly decreases to 3.8 %. This shows that L-ascorbic acid treatment significantly changes the surface chemistry of $Ti_3C_2T_x$, similar to the results in the report,[2] where Li-EDA treatment is shown to remove a significant amount of F termination from $Ti_3C_2T_x$. Figure 3b depicts a high-resolution peak of Ti2p ranging from 454.8 to 464.8 eV for Ti_3AlC_2 MAX phase (black), $Ti_3C_2T_x$ (red), and r-$Ti_3C_2T_x$ (blue). Deconvolution (Figure S1a and S1b, supporting information) shows that $Ti2p_{3/2}$ peaks appear between 454.8 to 459.0 eV and the peaks beyond 459.0 eV are their corresponding doublets ($Ti2p_{1/2}$). These peaks have been assigned to Ti, Ti^{2+}, Ti^{3+}, and Ti^{4+} chemical states as in the reports.[2,37,38] The peaks appearing at 454.8 eV (460.3 eV) and 459.0 eV (464.9 eV) for $Ti_3C_2T_x$ are assigned to Ti bonded to C of Ti_3C_2 crystal and TiO_2 resulting from surface oxidation, respectively.[37,38] For $Ti_3C_2T_x$, the component peak at 459.0 eV (464.9 eV) is also largely contributed by Ti^{4+} chemical states of Ti atoms surrounded by the O^{2-} ions in the lattice, which occurs due to the replacement of some carbons by oxygens in the crystal during the etching process.[2] This fact is supported by the increased intensity ratio of Ti^{4+} to Ti-C peaks for $Ti_3C_2T_x$ compared to Ti_3AlC_2 MAX phase. The peaks at 456.4 eV (461.5 eV) and 458.2 eV (263.5 eV) are assigned to Ti^{2+} and Ti^{3+} chemical states, respectively.[2,38,39] One of the main purposes of XPS analysis is to assess the difference between $Ti_3C_2T_x$ and r-$Ti_3C_2T_x$. Interestingly, we observed clear changes in the intensities of Ti^{3+} and Ti^{4+} components. In contrast

to $Ti_3C_2T_x$ (red), r-$Ti_3C_2T_x$ (blue) shows a high intensity of Ti^{3+} peak at 458.2 eV (463.7 eV) with a diminished Ti^{4+} peak at 459.0 eV (464.7 eV), indicating a reduction of Ti^{4+} chemical states to Ti^{3+} under L-ascorbic acid treatment.

The O1s fine spectra (Figure S1c and S1d, supporting information) of both $Ti_3C_2T_x$ and r-$Ti_3C_2T_x$ have been fitted with four different components peaking at 530.4, 531.6, 532.6, and 533.7 eV and are assigned to TiO_2, Ti-O, Ti-OH, and adsorbed H_2O molecules, respectively. The deconvolution clearly shows that TiO_2 component decreases upon reduction of $Ti_3C_2T_x$ with L-ascorbic acid, and center of gravity of O1s fine spectrum of r-$Ti_3C_2T_x$ is slightly shifted to higher energy with respect to $Ti_3C_2T_x$, consistent with the report.[2] Some changes can also be seen between C1s XPS spectra of $Ti_3C_2T_x$ and r-$Ti_3C_2T_x$ (see Figure S1e and S1f, supporting information). The C1s fine spectrum of $Ti_3C_2T_x$ has been deconvoluted into five components peaking at 282.4, 284.5, 285.6, 286.8, and 288.9 eV and are assigned to Ti-C bonds in $Ti_3C_2T_x$ crystal, C-C, CH_x, C-O, and COOH, respectively. The spectrum of r-$Ti_3C_2T_x$ has been deconvoluted with the same components, but peak intensity ratio of C bonds in the components; C-C, CH_x, C-O, and COOH altogether to that of Ti-C alone increases compared to $Ti_3C_2T_x$, similar to the results in the report.[2]

Figure 3c shows normalized Raman spectra of Ti_3AlC_2 MAX phase (black), $Ti_3C_2T_x$ (red), and r-$Ti_3C_2T_x$ (blue). Ti_3AlC_2 MAX phase shows six distinct Raman bands, among which three intense bands occurring at 180, 198, 268 cm^{-1} are associated with the vibrations of Ti and Al bonds and three shallow bands occurring at 575, 628, and 650 cm^{-1} are associated with Ti-C bonds.[1,40] A small peak at 149 cm^{-1} is the E_g vibrational mode of anatase phase TiO_2 particles[41] formed due to spontaneous oxidation of surface titanium atoms. Note that this peak is very intense relative to MXene bands intensity when there is a sufficient amount of TiO_2,[41] and hence even with a small amount present, it is easily detectable. $Ti_3C_2T_x$ and r-$Ti_3C_2T_x$ show a broadened peak at 205 cm^{-1},

which is assigned to the Ti-Al vibrational mode occurring at 198 cm^{-1} in MAX phase and is slightly blue-shifted, due to phonon stiffening effect as the crystals are thinned down to nano scale. Apparently, our observation suggests that this Raman peak is visible even at a small amount of Al in MXene crystals, which is below the detection limit of XPS. The three peaks occurring at 575, 628, and 650 cm^{-1} in MAX phase are merged and red-shifted in $Ti_3C_2T_x$ and r-$Ti_3C_2T_x$ as observed previously.[1,40]

XRD patterns (Figure 3d) show that several peaks are not observed in $Ti_3C_2T_x$ (red), including the most intense one appearing at 39.0° due to the disappearance of the non-basal crystal planes upon removal of Al layers by HF etching. Consistent with the reports,[1,28] we observed the broadening, loss of intensity, and shift of the peaks to lower angle for (00l) peaks such as (002) and (004). The peaks appearing in the range 33-45° broaden so significantly that they look merged together. A most prominent change is a huge shift of the (002) peak from 9.5° in Ti_3AlC_2 MAX to 6.5° in $Ti_3C_2T_x$, owing to the removal of Al layers and introduction of surface terminations (-F, -O, -OH).[36] r-$Ti_3C_2T_x$ shows similar XRD peaks to $Ti_3C_2T_x$, except that (002) peak is further shifted to a slightly lower angle, 6.0° in r-$Ti_3C_2T_x$, which could be attributed to further increase of the c-lattice spacing upon removal of F terminations.

3.2. Enhanced Electrical Conductivity of r-$Ti_3C_2T_x$

Figure 4a shows an SEM micrograph of r-$Ti_3C_2T_x$ with Ti/Au contact pads. More detailed images of $Ti_3C_2T_x$ and r-$Ti_3C_2T_x$ are presented in Figure S2, supporting information. High magnification SEM images of the $Ti_3C_2T_x$ and r-$Ti_3C_2T_x$ films are presented in the insets of Figure 4b and 4c, respectively. Figure 4b and 4c present the plots of the measured total resistance vs contact pad spacing for $Ti_3C_2T_x$ and r-$Ti_3C_2T_x$, respectively. Neglecting the small value of contact pad to probe resistance ($\sim 12\ \Omega$) measured in our case, we have used the following relation for

total measured resistance: $R_T = (^{R_s}/_W)L + 2R_c$, where R_s is the sheet resistance of the films, L and W are spacing and width of the metal pads, respectively, and R_c is the metal pad to MXene film contact resistance. Hence, from slopes of the fitted lines in Figures 4b and 4c, we obtained sheet resistance values as 1415 ± 125 and 288 ± 27 Ω/sq for $Ti_3C_2T_x$ and r-$Ti_3C_2T_x$, respectively. With the measured thicknesses as 1.5 and 1.2 µm for $Ti_3C_2T_x$ and r-$Ti_3C_2T_x$ films (see Figure S3, supporting information), the corresponding conductivity values are 471 ± 49 and 2819 ± 306 S/m, respectively. The contact resistance of Ti/Au pad with MXene films obtained from the y-intercept values in Figures 4b and 4c are 4.2 ± 0.4 and 0.5 ± 0.05 $K\Omega$ for $Ti_3C_2T_x$ and r-$Ti_3C_2T_x$ films, respectively, and the corresponding contact resistivities are $(2.6 \pm 0.3)x10^{-4}$ and $(3.3 \pm 0.4)x10^{-5}$ Ωm^2. These values are high compared to the values for continuous graphene-metal contacts,[42,43] but reasonable considering nature of the films made by drop casting of the MXene sheets.

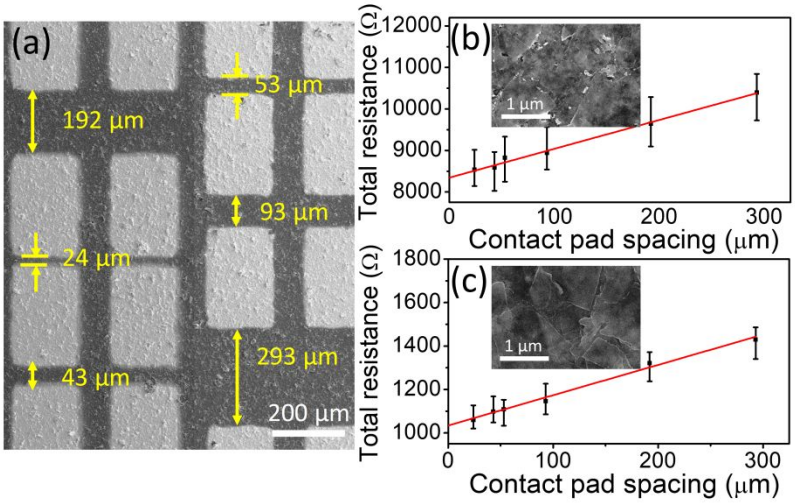

Figure 4. SEM image of Au/Ti contact pads on r-$Ti_3C_2T_x$ films on SiO_2/Si (a), Plots of total resistance vs contact pad spacing of (b) $Ti_3C_2T_x$ and (c) r-$Ti_3C_2T_x$ films on SiO_2/Si. Insets in Figures b and c are the high magnification SEM images of the corresponding films.

Although our conductivity values for $Ti_3C_2T_x$ and r-$Ti_3C_2T_x$ films fall within a widely scattered values of 2D titanium carbide MXene films reported previously,[16,24,33,37,44,45] these values are smaller than most of the previously reported values for $Ti_3C_2T_x$. Since, the conductivity of MXene films is synthesis and processing dependent, the relatively small electrical conductivity of our $Ti_3C_2T_x$ can mainly be attributed to the use of HF as an etchant instead of a mixture of HCl and alkali metal fluoride salts such as LiF, as suggested in the report[36]. Moreover, the choice of intercalant for delamination, flake size and thickness, and film processing method could also alter the conductivity. Most importantly, it is exciting to know that electrical conductivity of $Ti_3C_2T_x$ is enhanced six-fold upon treatment with L-ascorbic acid, suggesting a great value of the reduction process in MXene processing. Our result suggests that reduction of $Ti_3C_2T_x$ via L-ascorbic treatment significantly enhances the electrical conductivity regardless of the initial conductivity value. An eight-fold reduction in the contact resistivity of r-$Ti_3C_2T_x$ with respect to $Ti_3C_2T_x$ also suggests that r-$Ti_3C_2T_x$ is more suitable material than $Ti_3C_2T_x$ for fabricating devices that require metal-MXene contacts, such as for electronic and optoelectronic devices. The reason for the enhanced conductivity in r-$Ti_3C_2T_x$ can be explained as a consequence of the changes in chemistry of the MXene crystals during HF and L-ascorbic acid treatments. First, the carbon atoms that are replaced by O^{-2} ions during the HF etching process,[2] are subsequently removed by L-ascorbic acid treatment creating vacancies in the crystal lattice and provides a localized electron in the vacant site. Next, XPS result shows that a significant loss of fluorine terminations occurs during the reduction process. These modifications in the crystal chemistry cause redistribution of the missing hybridized Ti3d-C2p and Ti3d-F2p states to Ti-Ti metallic bond states near Fermi energy, thereby increasing the DOS at the Fermi level. With this argument, a significantly large electrical conductivity of each r-$Ti_3C_2T_x$ nanosheet is expected compared to an untreated $Ti_3C_2T_x$ sheet.

3.3 Oxidation Stability

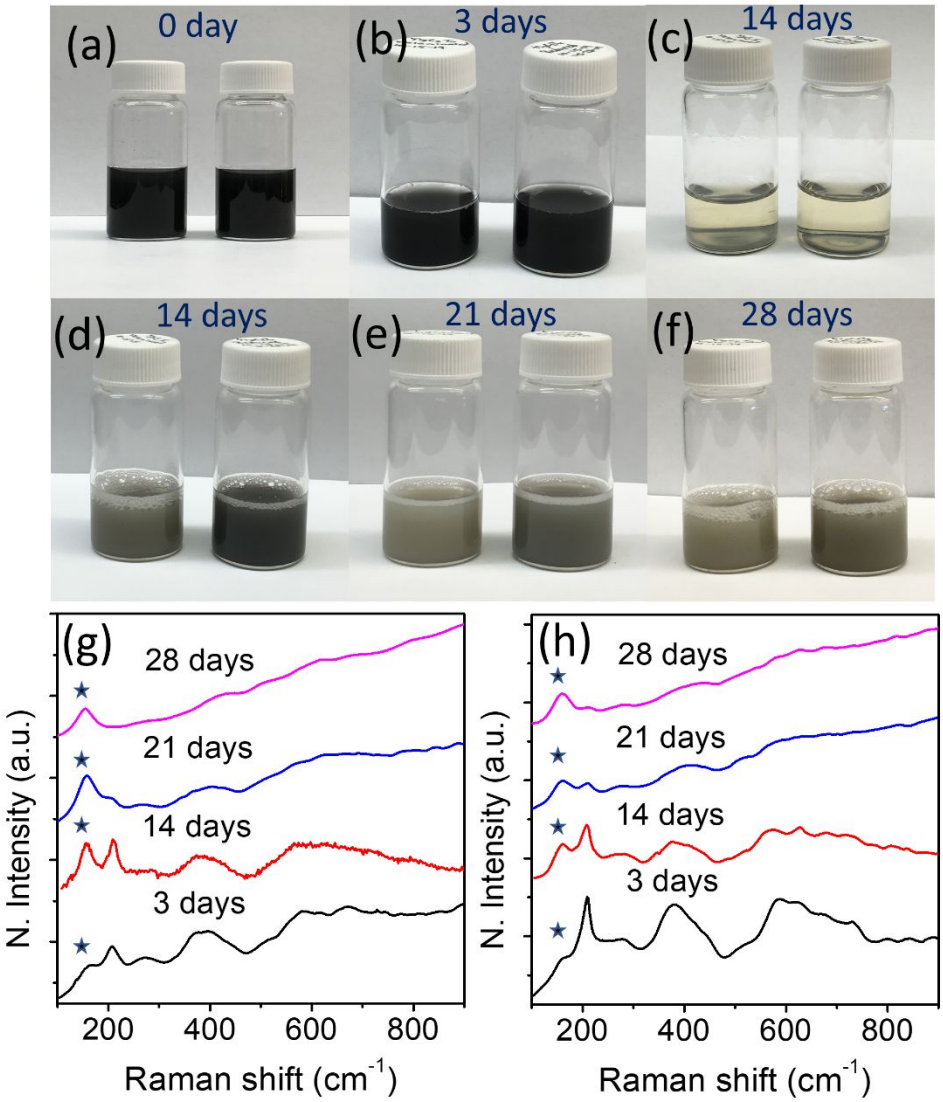

Figure 5. Photographs of the aqueous solutions of $Ti_3C_2T_x$ (left) and r-$Ti_3C_2T_x$ (right) collected after (a) 0 day, (b) 3 days, (c) 14 days before shaking, (d) 14 days, (e) 21 days, and (f) 28 days. The concentrations of $Ti_3C_2T_x$ and r-$Ti_3C_2T_x$ solutions were 15 mg in 10 ml of water. Normalized Raman spectra collected on dried powder from the aqueous solutions of (g) $Ti_3C_2T_x$, and (h) r-$Ti_3C_2T_x$ kept for different days.

Figures 5 (a-f) show photographs of the aqueous solutions of $Ti_3C_2T_x$ (left) and r-$Ti_3C_2T_x$ (right) collected on different days. We reiterate that the aqueous solutions (15 mg/10 ml) of $Ti_3C_2T_x$ and r-$Ti_3C_2T_x$ were prepared by re-dispersing the dried powders of the corresponding materials in water to study oxidation stability. Both of $Ti_3C_2T_x$ and r-$Ti_3C_2T_x$ aqueous solutions look black initially, but upon exposure to water for several days, $Ti_3C_2T_x$ aqueous solution turns whitish faster than r-$Ti_3C_2T_x$ aqueous solution, indicating a faster degradation of $Ti_3C_2T_x$ crystals. The repeated experiment with a lower concentration (5 mg/10 ml) of $Ti_3C_2T_x$ and r-$Ti_3C_2T_x$ in water results the same (see Figure S4, supporting information). As shown in Figure 5b, the MXene nanosheets allowed to oxidize for 3 days do not look distinctively different to eye, but the difference can easily be detected by Raman spectroscopic analysis of the corresponding dried powders (Figures 5g and 5h). The features in the Raman spectra in each of $Ti_3C_2T_x$ and r-$Ti_3C_2T_x$ exposed to water for a different length of time are different. With the increased number of days, the degraded MXene powders show a gradual increase of the E_g vibrational band intensity of anatase TiO_2 occurring at ~149 cm^{-1} (indicated with stars) and decrease of the MXene peak occurring at ~205 cm^{-1} as observed by Zhang et al.[31] It is evident from Figures 5g and 5h that the ratio of anatase TiO_2 to MXene band intensities increases faster for $Ti_3C_2T_x$ than r-$Ti_3C_2T_x$, which indicates that r-$Ti_3C_2T_x$ nanoflakes are more stable in oxygen-rich environment such as water. SEM micrographs (Figure S5, supporting information) further confirm that nucleation and growth of TiO_2 nanoparticles take place faster on $Ti_3C_2T_x$ surfaces than on r-$Ti_3C_2T_x$ surfaces.

It is evident that after treatment with L-ascorbic acid, $Ti_3C_2T_x$ nanosheets become more stable in oxygen rich environment. This result is consistent with a recent work,[30] which uncovered that $Ti_3C_2T_x$ nanosheets were protected from severe oxidation up to six months when stored in a sodium ascorbate aqueous solution. The average lateral size of the $Ti_3C_2T_x$ and r-$Ti_3C_2T_x$

nanosheets on the SEM images in Figure S2 c,d and S5 presented in supporting file are ~1.6 and ~1.5 μm, respectively. Hence, a faster degradation of $Ti_3C_2T_x$ nanosheets compared to r-$Ti_3C_2T_x$ in water is not because of the smaller flake size as reported previously.[31] The enhanced oxidation stability of the r-$Ti_3C_2T_x$ can be explained based on the reduction of the $Ti_3C_2T_x$ nanosheets caused by L-ascorbic acid molecules. As described above, O^{2-} ions replace a significantly large number of carbons from the $Ti_3C_2T_x$ lattice during the Al layer etching process as shown in Figure 1b. These oxygen sites in the $Ti_3C_2T_x$ crystal act as nucleation centers for TiO_2 nanoparticle growth. Upon exposure of the $Ti_3C_2T_x$ nanosheets to water, reactive oxygen species, such as hydroxyl radical or oxygen molecules react with the nanosheets breaking the Ti-C bonds and form Ti-O bonds.[30] This process accelerates the TiO_2 nanoparticle growth. The carbons released during this process are bonded to each other forming disordered carbon material (see Figure S6, supporting information). Hence, the MXene nanosheets continue to degrade while TiO_2 nanoparticles continue to increase in size. This argument is supported by SEM micrographs (see Figure S5, supporting information) of the MXene sheets, where TiO_2 nanoparticles are observed to increase in size with continued exposure to water. The TiO_2 nanoparticles growth on MXene surface also confirm that MXene degradation not only starts at the $Ti_3C_2T_x$ sheet edges as claimed in the reports,[30,31] but also occurs simultaneously at the basal plane. However, L-ascorbic acid treatment on $Ti_3C_2T_x$ removes the O^{2-} ions sitting in the carbon sites, and the possible nucleation sites for TiO_2 particle growth are minimized. This argument is supported by a much smaller density and size of the TiO_2 nanoparticles growth on the basal plane of r-$Ti_3C_2T_x$ compared to $Ti_3C_2T_x$ (see Figure S5, supporting information). Such an enhanced oxidation stability makes r-$Ti_3C_2T_x$ a promising material for use in applications.

3.4 SERS Activity

Figures 6a, 6b, and 6c show SERS spectra of the probe molecules, crystal violet (CV) at $2x10^{-6}$ M, methylene blue (MB) at $1x10^{-6}$ M, and rhodamine 6G (R6G) at $1x10^{-7}$ M, respectively, collected on $Ti_3C_2T_x/SiO_2/Si$ (black) and r-$Ti_3C_2T_x/SiO_2/Si$ (red) substrates. It is apparent that r-$Ti_3C_2T_x/SiO_2/Si$ substrate shows about an order of magnitude higher Raman signal intensity compared to $Ti_3C_2T_x/SiO_2/Si$ for all the three probe molecules. Raman enhancement on SERS substrates prepared with $Ti_3C_2T_x$ and r-$Ti_3C_2T_x$ on PVDF filter membrane (see photographs Figure S7, supporting information) showed similar results.

Table 1. Calculated analytical Raman enhancement factors for CV, MB, and R6G

Probe molecules	SERS substrates	Raman shift (cm^{-1})	Peak assignment	Dye concentration (M)	EF
CV	$Ti_3C_2T_x/SiO_2/Si$	1613	In-plane stretching of C-C ring[46]	$2.0x10^{-6}$	2.1×10^5
	r-$Ti_3C_2T_x/SiO_2/Si$				1.6×10^6
MB	$Ti_3C_2T_x/SiO_2/Si$	1623	In-plane stretching of C-C ring[47]	$1.0x10^{-6}$	1.0×10^5
	r-$Ti_3C_2T_x/SiO_2/Si$				7.8×10^5
R6G	$Ti_3C_2T_x/SiO_2/Si$	1361	carboxylate stretches[48]	$1.0x10^{-7}$	1.3×10^6
	r-$Ti_3C_2T_x/SiO_2/Si$				1.0×10^7

The SERS EF was calculated using the following equation: $EF = (I_{SERS}/C_{SERS})/(I_{ref}/C_{ref})$, where I_{SERS} is the Raman intensity of a selected vibrational mode of a dye with a concentration of C_{SERS}, and I_{ref} is the intensity of the same vibrational mode of the

dye on SERS inactive substrate (SiO_2/Si) with a concentration of C_{ref}. The calculated SERS EFs for different dyes are presented in Table 1.

It is evident that SERS EF is an order of magnitude higher on r-$Ti_3C_2T_x$/SiO_2/Si than on $Ti_3C_2T_x$/SiO_2/Si for all three dyes used. The calculated SERS EFs for $Ti_3C_2T_x$/SiO_2/Si are similar to that of the SERS substrates fabricated with $Ti_3C_2T_x$ on glass and silicon in the report[20] and are much larger than Ti_2NT_x-based SERS substrates fabricated on glass and silicon reported by Soundiraraju et al.[4]

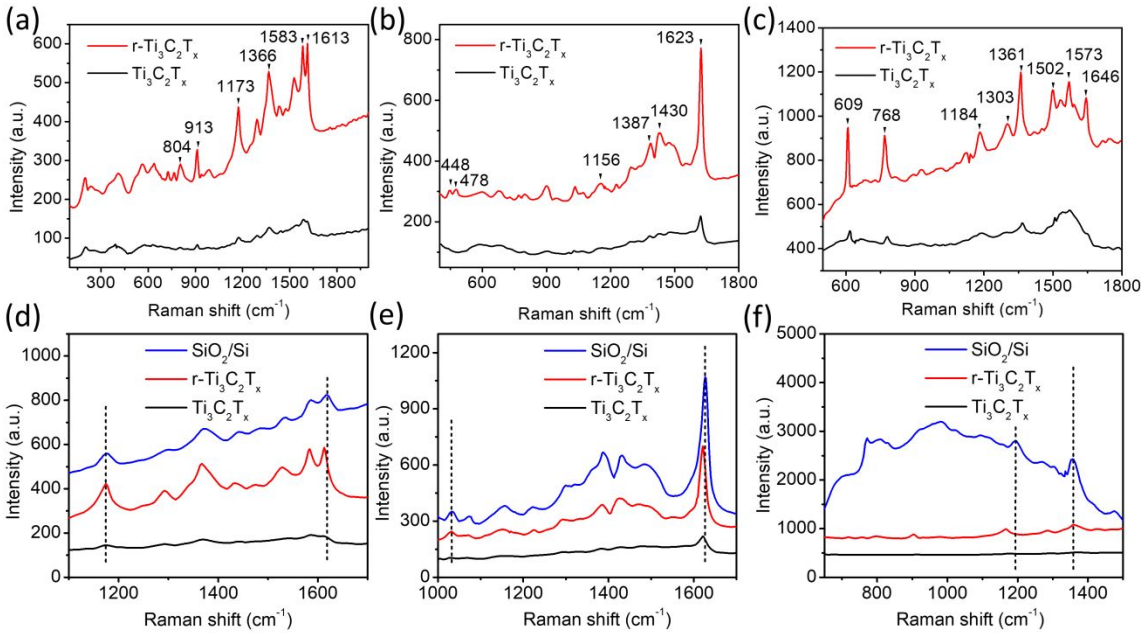

Figure 6. SERS spectra of (a, d) CV, (b, e) MB, and (c, f) R6G collected on $Ti_3C_2T_x$/SiO_2/Si (black) and r-$Ti_3C_2T_x$/SiO_2/Si (red), and bare SiO_2/Si (blue) substrates. Concentration of dyes on SiO_2/Si substrate is 1 M in water.

As shown in Figures 6d, 6e, and 6f, some of the vibrational peak positions in the SERS spectra of CV, MB, and R6G are red-shifted with respect to their original positions, i.e., Raman

peak positions measured on non-SERS substrate, SiO_2/Si. For example; in-plane stretching mode of C-C ring of CV and MB appear at 1619 and 1629 cm^{-1} on SiO_2/Si, respectively, which shift to 1613 and 1623 cm^{-1} on MXene substrates. For R6G, peak associated with the in-plane stretching mode of C-C ring appears at 1196 cm^{-1} on bare SiO_2/Si which is shifted to 1187 cm^{-1} on MXene substrates. We also noticed that there was no shift in some peaks, such as those appearing at 1173 cm^{-1} and 1032 cm^{-1} corresponding to in-plane bending mode of C-H in CV[46] and MB,[47] respectively, and 1361 cm^{-1} corresponding to carboxylate stretch mode[48] in R6G. The shift in the peak positions of dye molecules on $Ti_3C_2T_x$ and r-$Ti_3C_2T_x$ SERS substrates are attributed to charge transfer interaction[49,50] of the MXenes with the probe molecules. To understand our results, it is reasonable to expect the transfer of electrons from electron rich MXenes to C-C rings of the dye molecules, which slightly weakens C-C bonds of the rings, causing red-shift of the associated vibrational peaks. However, no charge transfer from MXenes to C-H bond of CV and MB, and to carboxylate group of R6G takes place. Hence, a peak shift associated with these bonds were not observed. Band shift due to charge transfer interaction is common in several other spectroscopies, such as XPS,[51] nuclear magnetic resonance spectroscopy,[52] and infrared absorption spectroscopy (IR).[52,53] In Raman spectroscopy, the degree of charge transfer is reflected by the magnitude of wavenumber shift[53,54] and has a positive correlation with Raman signal enhancement.[55] Hence, based on the magnitude of the band shift, the degree of the charge transfer is found to be slightly greater in R6G than in CV and MB. It is supported by the higher Raman EF of R6G compared to those of CV and MB. Moreover, the laser excitation wavelength, 532 nm is much closer to the light absorption peak position of R6G (527 nm) (see Figure S8 for UV visible spectra, supporting information) than the absorption peak positions of CV (591 nm) and MB (663 nm). Hence, the

matching of the excitation beam energy with molecular transition is another factor that accounts for higher EF of R6G than those of CV and MB.

Now, we discuss briefly to answer why r-$Ti_3C_2T_x$/SiO_2/Si SERS substrate enhances Raman signal of dye molecules more than $Ti_3C_2T_x$/SiO_2/Si substrate. As mentioned above, L-ascorbic acid treatment removes more than 50% of the F terminations on $Ti_3C_2T_x$ exposing a much larger number of surface-Ti atoms to the adsorbing dye molecules. This allows a larger population of adsorbing dye molecules to interact and form charge transfer complexes with r-$Ti_3C_2T_x$. Consequently, a higher EF factor is achieved. Additionally, as described above, the increased electronic DOS at the Fermi level in r-$Ti_3C_2T_x$ facilitates electronic charge transfer to dye molecules, causing an enhanced Raman EF. Despite increased metallic property or DOS at the Fermi level in r-$Ti_3C_2T_x$, no any plasmonic absorption was observed in the UV visible spectrum (see Figure S9, supporting information). Hence, the observed SERS enhancement of the dye molecules cannot be attributed directly to the electromagnetic contribution.

CONCLUSIONS

We have developed a facile and green protocol for room temperature synthesis of reduced $Ti_3C_2T_x$ MXene nanosheets via a simple treatment with L-ascorbic acid. The results show that r-$Ti_3C_2T_x$ has a 6-fold higher electrical conductivity and has a better oxidation stability than $Ti_3C_2T_x$, making r-$Ti_3C_2T_x$ a more promising material for most applications. Furthermore, r-$Ti_3C_2T_x$ offers a much smaller contact resistance with Ti/Au contact pads, which encourages the use of r-$Ti_3C_2T_x$ in fabricating devices that require metal-MXene contacts, such as electronic and optoelectronic devices.

The study demonstrates that r-$Ti_3C_2T_x$ enhances Raman signal of dye molecules by an order of magnitude higher than $Ti_3C_2T_x$. SERS enhancement factor obtained for R6G on r-$Ti_3C_2T_x$ is as high as 10^7 using the laser excitation wavelength of 532 nm, indicating a potential use of r-$Ti_3C_2T_x$ for making practical SERS substrates. The outstanding SERS activity of r-$Ti_3C_2T_x$ has been attributed to a larger number of Ti atoms exposed due to the loss of F terminations for allowing a larger population of dye molecules to interact with r-$Ti_3C_2T_x$. The higher SERS activity of r-$Ti_3C_2T_x$ is further re-enforced by increased electronic DOS at the Fermi level. The findings of this study suggest that reduced MXene could be a superior choice over MXene prepared by regular methods, especially for the applications that employ high electronic conductivity, such as electrode materials for batteries and supercapacitors, photodetectors, and SERS-based sensors.

ASSOCIATED CONTENT

Supporting Information. Deconvolution of XPS fine peaks for Ti2p, O1s, and C1s; Details of electrical measurements; Calculation of Electrical conductivity and contact resistivity; Thickness Measurement for $Ti_3C_2T_x$ and r-$Ti_3C_2T_x$ films; MXene oxidation stability test; SEM analysis of degraded $Ti_3C_2T_x$ and r-$Ti_3C_2T_x$; Raman spectra of disordered carbon material formed on MXene; Photographs of the SERS substrates on PVDF filter membranes; UV-vis absorption spectra of CV, MB, and R6B; Examination of plasmonic absorption in $Ti_3C_2T_x$ and r-$Ti_3C_2T_x$

AUTHOR INFORMATION

Corresponding Author

*Fei Yan (fyan@nccu.edu), Tej B. Limbu (tejblimbu@gmail.com)

Notes

The authors declare no competing financial interest.

ACKNOWLEDGMENT

The authors are grateful for the financial support of this project by the U.S. National Science Foundation (Awards # 1831133 and #1523617). Q. L. and S. K. would like to thank NSF Award #1905833 and DOE FG02-08ER46531. This work was performed in part at the Analytical Instrumentation Facility (AIF) and Nanofabrication facility (NNF) at North Carolina State University, which is supported by the State of North Carolina and the National Science Foundation (award number ECCS-1542015). The AIF and NNF are members of the North Carolina Research Triangle Nanotechnology Network (RTNN), a site in the National Nanotechnology Coordinated Infrastructure (NNCI). The authors thank Dr. Spyridon Pavlidis and Mr. Rohan Sengupta for assisting in electrical measurements.

ABBREVIATIONS

2D, two-dimensional; TMAOH, tetramethylammonium hydroxide; Li-EDA Li-ethylenediamine; r-$Ti_3C_2T_x$, reduced $Ti_3C_2T_x$ MXene; CV, crystal violet; MB, methylene blue; R6G, rhodamine 6G; SERS, surface-enhanced Raman scattering; AFM, atomic force microscopy; SEM, scanning electron microscopy; TEM, transmission electron microscopy; SAED, selected area electron diffraction; XPS, X-ray photoelectron spectroscopy; XRD, X-ray diffractometry.

REFERENCES

[1] M. Naguib, M. Kurtoglu, V. Presser, J. Lu, J. Niu, M. Heon, L. Hultman, Y. Gogotsi, and M.W. Barsoum, Adv. Mater., 2011, **23**, 4248.

[2] Y. Yoon, T.A. Le, A.P. Tiwari, I. Kim, M.W. Barsoum, and H. Lee, Nanoscale, 2018, **10**, 22429.

[3] K. Chaudhuri, M. Alhabeb, Z. Wang, V.M. Shalaev, Y. Gogotsi, and A. Boltasseva, ACS Photonics, 2018, **5**, 1115.

[4] B. Soundiraraju and B.K. George, ACS Nano, 2017, **11**, 8892.

[5] M.H. Tran, T. Schäfer, A. Shahraei, M. Dürrschnabel, L. Molina-Luna, U.I. Kramm, and C.S. Birkel, ACS Appl. Energy Mater., 2018, **1**, 3908.

[6] J.L. Hart, K. Hantanasirisakul, A.C. Lang, B. Anasori, D. Pinto, Y. Pivak, J.T. van Omme, S.J. May, Y. Gogotsi, and M.L. Taheri, Nat Commun, 2019, **10**, 522.

[7] L. Verger, V. Natu, M. Carey, and M.W. Barsoum, Trends in Chemistry, 2019, S2589597419300978.

[8] M. Naguib, O. Mashtalir, J. Carle, V. Presser, J. Lu, L. Hultman, Y. Gogotsi, and M.W. Barsoum, ACS Nano, 2012, **6**, 1322.

[9] M. Khazaei, M. Arai, T. Sasaki, C.-Y. Chung, N.S. Venkataramanan, M. Estili, Y. Sakka, and Y. Kawazoe, Advanced Functional Materials, 2013, **23**, 2185.

[10] M.R. Lukatskaya, O. Mashtalir, C.E. Ren, Y. Dall'Agnese, P. Rozier, P.L. Taberna, M. Naguib, P. Simon, M.W. Barsoum, and Y. Gogotsi, Science, 2013, **341**, 1502.

[11] M. Ghidiu, M.R. Lukatskaya, M.-Q. Zhao, Y. Gogotsi, and M.W. Barsoum, Nature, 2014, **516**, 78.

[12] Q. Pan, C. Duan, H. Liu, M. Li, Z. Zhao, D. Zhao, Y. Duan, Y. Chen, and Y. Wang, ACS Appl. Energy Mater., 2019, **2**, 6834.

[13] G. Gao, A.P. O'Mullane, and A. Du, ACS Catal., 2017, **7**, 494.

[14] Z.W. Seh, K.D. Fredrickson, B. Anasori, J. Kibsgaard, A.L. Strickler, M.R. Lukatskaya, Y. Gogotsi, T.F. Jaramillo, and A. Vojvodic, ACS Energy Lett., 2016, **1**, 589.

[15] C.E. Ren, K.B. Hatzell, M. Alhabeb, Z. Ling, K.A. Mahmoud, and Y. Gogotsi, J. Phys. Chem. Lett., 2015, **6**, 4026.

[16] C. (John) Zhang, B. Anasori, A. Seral-Ascaso, S.-H. Park, N. McEvoy, A. Shmeliov, G.S. Duesberg, J.N. Coleman, Y. Gogotsi, and V. Nicolosi, Advanced Materials, 2017, **29**, 1702678.

[17] G. Ying, A.D. Dillon, A.T. Fafarman, and M.W. Barsoum, Mat. Research Lett., 2017, **5**, 391.

[18] J. Liu, H.-B. Zhang, R. Sun, Y. Liu, Z. Liu, A. Zhou, and Z.-Z. Yu, Advanced Materials, 2017, **29**, 1702367.

[19] D.B. Velusamy, J.K. El-Demellawi, A.M. El-Zohry, A. Giugni, S. Lopatin, M.N. Hedhili, A.E. Mansour, E.D. Fabrizio, O.F. Mohammed, and H.N. Alshareef, Advanced Materials, 2019, **31**, 1807658.

[20] A. Sarycheva, T. Makaryan, K. Maleski, E. Satheeshkumar, A. Melikyan, H. Minassian, M. Yoshimura, and Y. Gogotsi, J. Phys. Chem. C, 2017, **121**, 19983.

[21] E. Satheeshkumar, T. Makaryan, A. Melikyan, H. Minassian, Y. Gogotsi, and M. Yoshimura, Scientific Reports, 2016, **6**, 32049.

[22] K. Hantanasirisakul, M. Alhabeb, A. Lipatov, K. Maleski, B. Anasori, P. Salles, C. Ieosakulrat, P. Pakawatpanurut, A. Sinitskii, S.J. May, and Y. Gogotsi, Chem. Mater., 2019, **31**, 2941.

[23] R. Li, L. Zhang, L. Shi, and P. Wang, ACS Nano, 2017, **11**, 3752.

[24] Z. Ling, C.E. Ren, M.-Q. Zhao, J. Yang, J.M. Giammarco, J. Qiu, M.W. Barsoum, and Y. Gogotsi, Proc Natl Acad Sci USA, 2014, **111**, 16676.

[25] Y. Xie and P.R.C. Kent, Phys. Rev. B, 2013, **87**, 235441.

[26] M. Savchak, N. Borodinov, R. Burtovyy, M. Anayee, K. Hu, R. Ma, A. Grant, H. Li, D.B. Cutshall, Y. Wen, G. Koley, W.R. Harrell, G. Chumanov, V. Tsukruk, and I. Luzinov, ACS Appl. Mater. Interfaces, 2018, **10**, 3975.

[27] Y. Chen, K. Fu, S. Zhu, W. Luo, Y. Wang, Y. Li, E. Hitz, Y. Yao, J. Dai, J. Wan, V.A. Danner, T. Li, and L. Hu, Nano Lett., 2016, **16**, 3616.

[28] X. Xie, Y. Zhu, F. Li, X. Zhou, and T. Xue, Sci. China Technol. Sci., 2019, **62**, 1202.

[29] K. Kneipp, Y. Wang, H. Kneipp, L.T. Perelman, I. Itzkan, R.R. Dasari, and M.S. Feld, Phys. Rev. Lett., 1997, **78**, 1667.

[30] X. Zhao, A. Vashisth, E. Prehn, W. Sun, S.A. Shah, T. Habib, Y. Chen, Z. Tan, J.L. Lutkenhaus, M. Radovic, and M.J. Green, Matter, 2019, **1**, 513.

[31] C.J. Zhang, S. Pinilla, N. McEvoy, C.P. Cullen, B. Anasori, E. Long, S.-H. Park, A. Seral-Ascaso, A. Shmeliov, D. Krishnan, C. Morant, X. Liu, G.S. Duesberg, Y. Gogotsi, and V. Nicolosi, Chem. Mater., 2017, **29**, 4848.

[32] T. Habib, X. Zhao, S.A. Shah, Y. Chen, W. Sun, H. An, J.L. Lutkenhaus, M. Radovic, and M.J. Green, Npj 2D Mater Appl, 2019, **3**, 8.

[33] A. Lipatov, M. Alhabeb, M.R. Lukatskaya, A. Boson, Y. Gogotsi, and A. Sinitskii, Adv. Electron. Mater., 2016, **2**, 1600255.

[34] H. Ghassemi, W. Harlow, O. Mashtalir, M. Beidaghi, M.R. Lukatskaya, Y. Gogotsi, and M.L. Taheri, J. Mater. Chem. A, 2014, **2**, 14339.

[35] V. Natu, J.L. Hart, M. Sokol, H. Chiang, M.L. Taheri, and M.W. Barsoum, Angewandte Chemie International Edition, 2019, **58**, 12655.

[36] M. Alhabeb, K. Maleski, B. Anasori, P. Lelyukh, L. Clark, S. Sin, and Y. Gogotsi, Chem. Mater., 2017, **29**, 7633.

[37] A. Pazniak, P. Bazhin, N. Shplis, E. Kolesnikov, I. Shchetinin, A. Komissarov, J. Polcak, A. Stolin, and D. Kuznetsov, Materials & Design, 2019, **183**, 108143.

[38] J. Halim, KM Cook, M. Naguib, P. Eklund, Y. Gogotsi, Y. Rosen, J. Barsoum, Applied Surface Science., 2016, **30**, 406-17.

[39] Y. Zhang, Z. Xing, X. Liu, Z. Li, X. Wu, J. Jiang, M. Li, Q. Zhu, and W. Zhou, ACS Appl. Mater. Interfaces, 2016, **8**, 26851.

[40] V. Presser, M. Naguib, L. Chaput, A. Togo, G. Hug, and M.W. Barsoum, Journal of Raman Spectroscopy, 2012, **43**, 168.

[41] O. Frank, M. Zukalova, B. Laskova, J. Kürti, J. Koltai, and L. Kavan, Phys. Chem. Chem. Phys., 2012, **14**, 14567.

[42] S. Min Song, T. Yong Kim, O. Jae Sul, W. Cheol Shin, and B. Jin Cho, Appl. Phys. Lett., 2014, **104**, 183506.

[43] V. Passi, A. Gahoi, E.G. Marin, T. Cusati, A. Fortunelli, G. Iannaccone, G. Fiori, and M.C. Lemme, Advanced Materials Interfaces, 2019, **6**, 1801285.

[44] J. Halim, M.R. Lukatskaya, K.M. Cook, J. Lu, C.R. Smith, L.-Å. Näslund, S.J. May, L. Hultman, Y. Gogotsi, P. Eklund, and M.W. Barsoum, Chem. Mater., 2014, **26**, 2374.

[45] H, Kitadai, X. Wang, N. Mao, S. Huang, X. Ling, J. Phys. Chem. Lett., 2019, **10**, 3043.

[46] L. Pei, Y. Huang, C. Li, Y. Zhang, B.A. Rasco, and K. Lai, J. Nanomaterials, 2014.

[47] K.-D. Shim and E.-S. Jang, Bulletin of the Korean Chemical Society, 2018, **39**, 936.

[48] M. Liu, M. Liu, Y. Shi, Y. Shi, G. Zhang, G. Zhang, Y. Zhang, M. Wu, J. Ren, and B. Man, Appl. Spectrosc., 2018, **72**, 1613.

[49] Y. Wang, W. Ji, H. Sui, Y. Kitahama, W. Ruan, Y. Ozaki, and B. Zhao, J. Phys. Chem. C, 2014, **118**, 10191.

[50] S. Liu, Y. Li, X. Zhao, X. Liu, and M. Chen, Spectrochimica Acta Part A: Molecular and Biomolecular Spectroscopy, 2011, **82**, 205.

[51] C. Lenser, Q. Lu, E. Crumlin, H. Bluhm, and B. Yildiz, J. Phys. Chem. C, 2018, **122**, 4841.

[52] M.S. Refat, H.A. Saad, A.M.A. Adam, M.A. Al-Omar, and A.M. Naglah, Acta Pharmaceutica, 2016, **66**, 533.

[53] T.B. Limbu, F. Mendoza, D. Barrionuevo, J. Carpena, B. Maruyama, R.S. Katiyar, B.R. Weiner, and G. Morell, AIP Advances, 2016, **6**, 035319.

[54] A.C. Crowther, A. Ghassaei, N. Jung, and L.E. Brus, ACS Nano, 2012, **6**, 1865.

[55] H. Kitadai, X. Wang, N. Mao, S. Huang, and X. Ling, J. Phys. Chem. Lett., 2019, **10**, 3043.

TOC Entry

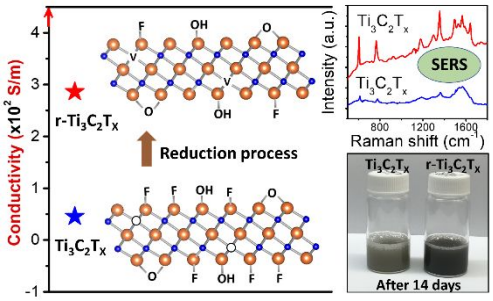

Surface engineering of ultrathin MXene nanosheets via L-ascorbic acid treatment under ambient conditions makes them more appealing for practical applications.